Nanoscale

REVIEW

View Article Online
View Journal | View Issue

Check for updates

Cite this: *Nanoscale*, 2025, **17**, 16988

Advancing electrocatalytic CO_2 reduction: key strategies for scaling up to industrial applications

Lei Wang and Yimin Wu *

Electrocatalytic CO_2 reduction (eCO_2RR) to high value-added C_{2+} products offers a highly promising pathway toward carbon neutrality and sustainable energy storage. However, the limited activity of current catalysts and the suboptimal configuration of reaction systems hinder the achievement of high C_{2+} selectivity and long-term operational stability, falling short of industrial application requirements. In this review, we take a unique perspective to examine recent advances in the functional design of catalysts and the optimization of reactor systems. We highlight that rational catalyst design can enhance C_{2+} product selectivity, while optimization of reactor components can improve system stability. The integration of innovative technologies with system-level optimization holds great potential to advance the scalability and economic feasibility of eCO_2RR. This review bridges the gap between fundamental research and industrial application of eCO_2RR, offering critical insights to guide its development as a practical and scalable technology.

Received 21st April 2025,
Accepted 20th June 2025

DOI: 10.1039/d5nr01624j

rsc.li/nanoscale

Open Access Article. Published on 23 June 2025. Downloaded on 4/15/2026 7:29:37 PM.
This article is licensed under a Creative Commons Attribution-NonCommercial 3.0 Unported Licence.

1. Introduction

Over the past few decades, rising CO_2 emissions from fossil fuel combustion have posed potential threats to the global climate, such as ocean acidification, extreme weather events, and droughts.[1,2] High concentrations of CO_2 can also lead to health risks and water security challenges.[3] The rapid increase in CO_2 emissions has prompted scientists and governments to collaborate on achieving net-zero emissions and developing efficient CO_2 conversion technologies. eCO_2RR into highly value-added chemicals and fuels using renewable energy is a promising method to reduce carbon emissions and support the development of a sustainable society.[4–7]

A typical CO_2 electrolyzer consists of a cathode chamber and an anode chamber separated by an ion exchange membrane. The eCO_2RR occurs at the cathode, while the oxygen evolution reaction (OER) usually occurs at the anode (Fig. 1).[8] CO_2, being a fully oxidized and thermodynamically stable molecule, poses several significant challenges for electrochemical conversion. Firstly, eCO_2RR is a thermodynamically uphill reaction with a high activation barrier, necessitating a sufficient overpotential to drive the reaction and make CO_2 conversion feasible.[9] Over 16 products have been reported from eCO_2RR, such carbon monoxide, methane, methanol, formate, ethylene, ethanol, acetate, and *n*-propanol.[10–13] Secondly, eCO_2RR involves multiple electron/proton transfer steps, with electrons and protons supplied by water.[14] This proton-assisted process involves various intermediates and products, complicating the control of product selectivity.[15] In aqueous electrolytes, the competing hydrogen evolution reaction (HER) can inhibit the formation of reduced products, further complicating eCO_2RR.[16] Therefore, achieving effective eCO_2RR relies on the rational design of catalysts to minimize side reactions and enhance selective production of reduced products.

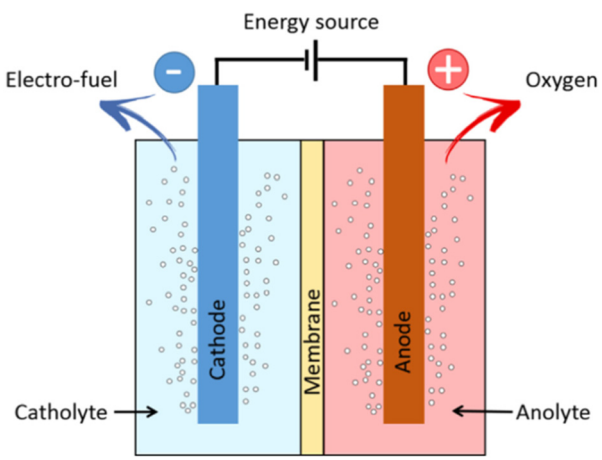

Fig. 1 A typical schematic of an ion-conducting membrane based CO_2 electrolyzer.[8] Reprinted with permission. Copyright 2016 Elsevier.

Department of Mechanical and Mechatronics Engineering, Waterloo Institute for Nanotechnology, Materials Interfaces Foundry, University of Waterloo, Waterloo, Ontario N2L 3G1, Canada. E-mail: yimin.wu@uwaterloo.ca

This journal is © The Royal Society of Chemistry 2025

Open Access Article. Published on 23 June 2025. Downloaded on 4/15/2026 7:29:37 PM. This article is licensed under a Creative Commons Attribution-NonCommercial 3.0 Unported Licence.

To date, only Cu-based catalysts have demonstrated the capability to efficiently convert CO_2 into valuable C_{2+} products *via* electrocatalysis. As a result, extensive research has focused on the rational design of Cu-based catalysts to achieve desirable activity and stability. In this review, we not only summarize the commonly adopted strategies for catalyst design, but also discuss the development of CO_2 electrolyzers ranging from laboratory-scale reactors to systems with industrial application potential. This review aims to provide an in-depth perspective on how to bridge the gap between fundamental research and scalable industrial implementation in the field of eCO_2RR.

2. Cu-based electrocatalyst

Among the state-of-the-art eCO_2RR catalysts, copper is the only metal capable of reducing CO_2 into hydrocarbons and alcohols.[17] Therefore, numerous approaches, including alloying,[18–22] oxide-derived copper (OD-Cu),[23–25] grain boundaries (GBs),[26,27] and morphology modification,[28–30] have been developed to increase the capability of the Cu-based catalysts. The main technique of these approaches is to create specific ensembles with controllable selectivity towards the targeted products (*e.g.* ethylene and methane). The revealed reaction mechanism and catalytic behaviors may further shine a light for development of Cu-based electrocatalysts.

2.1. Alloy effects

Single-metal catalysts often produce only C_1 (*e.g.*, CO, HCOOH) products (*e.g.*, Au, Sn and Bi) and suffer from undesirable HER (*e.g.*, Pt and Pd), or exhibit low product selectivity due to the diverse reaction pathways of Cu.[31–33] Consequently, many researchers have focused on alloying other metals with Cu. This approach aims to optimize the electronic structure and local coordination environment of Cu atoms, alter the adsorption strength of key intermediates, and expose new active sites, thereby enhancing the formation of multi-carbon products.[34,35] Additionally, bimetallic catalysts can enhance CO coverage on the catalyst surface, promoting C–C coupling towards C_{2+} products (*e.g.*, C_2H_4, and C_2H_5OH).[33] Therefore, alloying strategies play a crucial role in modulating the reaction pathways of eCO_2RR.[36]

The alloying effect on the formation mechanisms of C_1 and C_{2+} products is complex. Under severe cathodic conditions (*i.e.*, cathodic potentials > −1.1 V *vs.* reversible hydrogen electrode, RHE), CH_4 production tend to outcompete C_2H_4. This is because CH_4 formation requires a higher overpotential and faster kinetics.[37] In the CuAg alloy system, many studies reported CH_4 as the main reduced product. For instance, studies have shown that Ag–Cu surfaces, due to low-coordination sites, strongly bind with *CO, inhibiting CO–CO coupling and resulting in lower selectivity towards C_2H_4 (Fig. 2a and b).[38] Ag-modified Cu nanowires ($Cu_{68}Ag_{32}$) exhibit more than three times the CH_4 activity and selectivity compared to pristine Cu nanowires. *In situ* characterizations reveal that the dynamic reoxidation/reduction-driven atomic interdiffusion of Cu sites facilitates the CuAg alloying (Fig. 2c). The induced tensile strain strengthens the binding with *CHO intermediates, promoting further reduction and suppressing undesired HER.[39] Furthermore, as both Cu and Ag have valence d-states, the catalytic performance of CuAg catalysts is in principle determined by their electronic structure. The interface interaction between Cu and Ag alters the surface electronic structure and tailors the adsorption strength of *CO on the catalytic surface (Fig. 2d). Consequently, *CO tends to convert into CH_4 before desorbing from the Cu surface.[40] Conversely, for the CuAg alloy system that produces C_{2+} products, the CO_2 reduction pathway follows a tandem catalysis mechanism. Ag sites are more favorable for CO production, which enriches CO at neighboring Cu sites and promotes C–C coupling towards C_{2+} products such as ethylene and ethanol.[41,42] For example, Gewirth and co-workers reported that a CuAg alloy prepared by additive-controlled electrodeposition achieves 60% ethylene selectivity and 25% ethanol selectivity (Fig. 2e). The high selectivity for C_{2+} products results from the stabilization of the Cu_2O overlayer and optimization of CO intermediates availability at Cu sites through Ag doping in the alloy system.[18] Zheng and co-workers reported that the introducing Ag facilitates electron transfer from Cu to Ag, creating electron-deficient Cu sites. This enhances the adsorption of key intermediates in the ethanol reaction pathway, such as $*CH_3CHO$ and $*CH_3CH_2O$, resulting in excellent ethanol selectivity (Fig. 2f).[43]

Additionally, the mixing modes of bimetallic catalysts influence the product distribution in eCO_2RR. Kenis and co-workers demonstrated that phase-separated PdCu catalysts achieve the highest ethylene selectivity (~50%) compared to both ordered and disordered counterparts.[44] The lower d-band center of these phase-separated catalysts, compared to Cu NPs, indicates the weaker CO intermediate binding. This suggests that geometric and structural effects play a more significant role than electronic effects in enhancing product distribution.[44] Jaramillo and colleagues reported that gold nanoparticles on polycrystalline copper foil follow a tandem catalysis mechanism, showing superior synergistic catalytic activity and selectivity compared to gold, copper, and CuAg alloys.[45] In summary, alloying strategies open new avenues for enhancing the conversion of eCO_2RR to target products, but different structures and interfaces will give different electronic states for different products selectivity.

2.2. Oxidation states

Beyond alloying strategies, modulation of the oxidation state also affects the activity and selectivity of eCO_2RR. For oxide-derived Cu (OD-Cu), the oxidation state of the metal centers is effectively maintained by residual oxygen species on the surface or subsurface of the catalyst after *in situ* reduction. These oxidized Cu species serve as active sites for eCO_2RR, facilitating C–C coupling to form C_{2+} products. For example, plasma-oxidized Cu can achieve ethylene selectivity exceeding 60%.[46] Comparative experiments with various plasma treat-

Open Access Article. Published on 23 June 2025. Downloaded on 4/15/2026 7:29:37 PM.
This article is licensed under a Creative Commons Attribution-NonCommercial 3.0 Unported Licence.

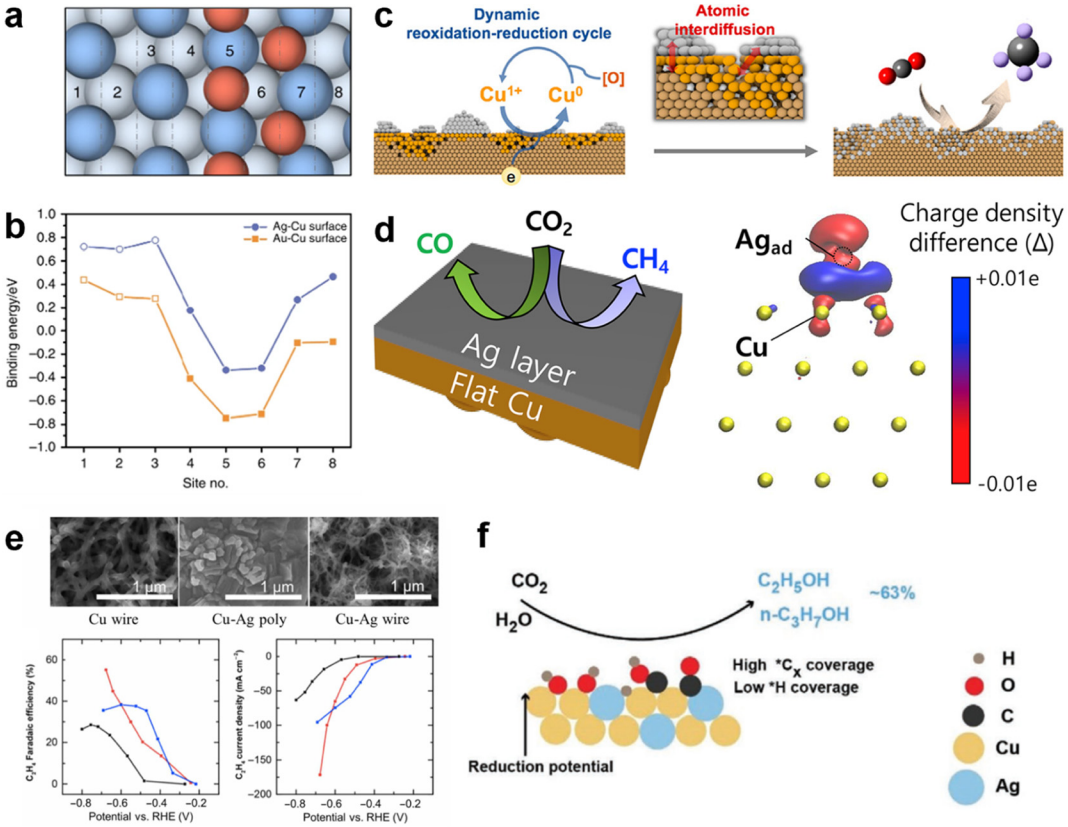

Fig. 2 Alloy effect of electrochemical CO_2 reduction. (a) Top view of the unit cell used for computational investigations (blue: top layer Ag or Au atoms; light blue: bottom layer Ag or Au atoms; orange: Cu atoms). The site numbers show the position and chemical environment of the binding sites.[38] Reprinted with permission. Copyright 2019 Springer Nature. (b) Energy diagram for CO adsorption on the Ag–Cu surface (blue line) and Au-Cu surface (orange line).[38] Reprinted with permission. Copyright 2019 Springer Nature. (c) The dynamic reoxidation/reduction-driven atomic interdiffusion processes of Cu sites.[39] Reprinted with permission. Copyright 2020 American Chemical Society. (d) The optimized Cu/Ag layered catalyst for eCO_2RR-to-CH_4 conversion.[40] Reprinted with permission. Copyright 2020 Elsevier. (e) The scanning electron microscopy (SEM) images and corresponding C_2H_4 FE of CuAg bimetallic electrocatalysts from additive-controlled electrodeposition.[18] Reprinted with permission. Copyright 2018 American Chemical Society. (f) Illustration of the eCO_2RR process on the Cu_3Ag_1 catalyst.[43] Reprinted with permission. Copyright 2020 WILEY-VCH Verlag GmbH & Co. KGaA, Weinheim.

ments confirm the crucial role of Cu^+ in the conversion of eCO_2RR to C_2H_4 (Fig. 3a).[46] Sargent and colleagues used *in situ* soft X-ray absorption spectroscopy to monitor the oxidation state of copper over time under eCO_2RR conditions.[47] The sol–gel materials effectively slow the electrochemical reduction of oxidized copper species, stabilizing Cu^+ species under cathodic potentials (Fig. 3b).[47] The catalyst achieves an ethylene partial current density of 160 mA cm^{-2} and an ethylene-to-methane ratio of 200 (Fig. 3c). However, after one hour of continuous operation, only 23% of Cu^+ species can be effectively preserved (Fig. 3b). Theoretical analyses have further explained why OD-Cu leads to the production of ethylene and ethanol. Research indicates that 4-(6-)coordinated Cu adatoms and $Cu_3^{\delta+}O_3$ leads to tethering CO_2, while metastable near-surface oxygen atoms in fcc-(111) or (100)-like Cu matrix promote C–C coupling, thereby enhancing the formation of C_{2+} products.[48] Nevertheless, the poor stability of oxidized $Cu^{\delta+}$ species under high current densities poses significant challenges for the widespread application of OD-Cu. To enhance the stability of oxidized $Cu^{\delta+}$ species, Fang and colleagues developed a one-step surface coordination method to synthesize ultrastable and hydrophobic $Cu^{\delta+}$, achieving a C_2 faradaic efficiency (FE) of 90.6% at a partial current density of 453.3 mA cm^{-2} (Fig. 3d and e). Spectroscopic and computational results indicate that Cu(II) carboxylate coordination species on the catalyst surface can effectively stabilize active $Cu^{\delta+}$ species.[49] Additionally, heteroatom doping can also stabilize $Cu^{\delta+}$ species. For example, the average oxidation state of copper can range from +0.25 to +0.78 by varying the boron doping content.[50] PDOS analysis shows that electron transfer from Cu to boron creates a negatively charged Cu site, increasing the formation energy of *CHO while lowering the reaction barrier for *CO dimerization (Fig. 3f). These findings provide new insights into enhancing the stability of active $Cu^{\delta+}$ species during eCO_2RR.

However, *in situ* reduction of OD-Cu can also cause morphological and structural changes, making the identification of its true active sites a subject of ongoing debate.[51–53] For instance, Cu^+, mixed oxidation states ($Cu^{\delta+}$) of Cu (*e.g.*, Cu^{2+}

 This journal is © The Royal Society of Chemistry 2025

Open Access Article. Published on 23 June 2025. Downloaded on 4/15/2026 7:29:37 PM.
This article is licensed under a Creative Commons Attribution-NonCommercial 3.0 Unported Licence.

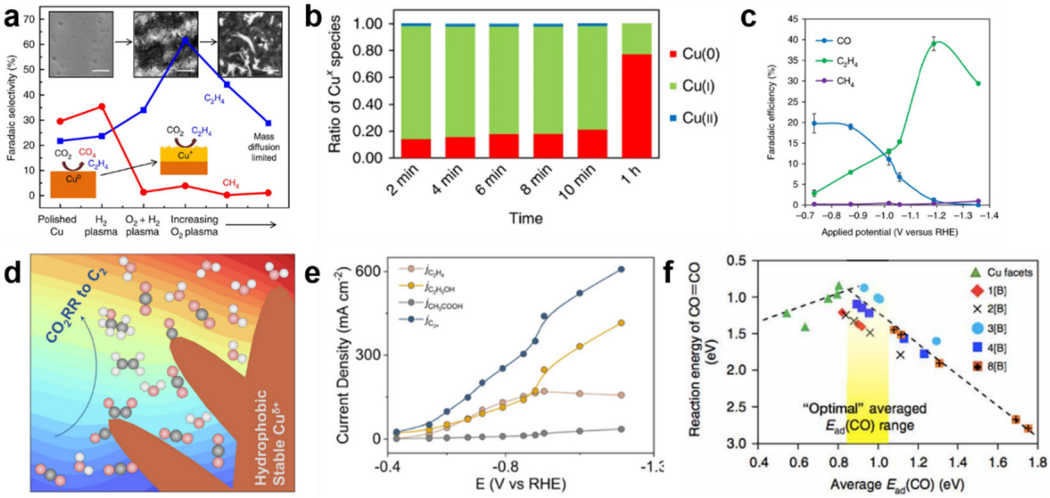

Fig. 3 Oxidation states manipulation for eCO_2RR. (a) Summary of the C_2H_4 selectivity of different plasma-activated Cu electrocatalysts.[46] Reprinted with permission. Copyright 2016 Springer Nature. (b) Ratio of Cu oxidation states relative to the reaction time at –1.2 V *vs.* RHE for electro-redeposited Cu.[47] Reprinted with permission. Copyright 2018 Springer Nature. (c) Reduced products of eCO_2RR on electro-redeposited Cu.[47] Reprinted with permission. Copyright 2018 Springer Nature. (d) Illustration of the eCO_2RR process on the ultrastable and hydrophobic $Cu^{\delta+}$ catalyst.[49] Reprinted with permission. Copyright 2023 American Chemical Society. (e) Current density distribution of the ultrastable and hydrophobic $Cu^{\delta+}$ catalyst.[49] Reprinted with permission. Copyright 2023 American Chemical Society. (f) Boron doping was able to change the average absorption energy of CO in the copper surface and lower the CO-CO dimerization energy.[50] Reprinted with permission. Copyright 2018 Springer Nature.

and Cu^+) or their interface have been identified as the active sites for promoting CO-CO coupling in OD-Cu during eCO_2RR.[46,54] Conversely, another study suggests that metallic Cu is the active site in bulk Cu catalysts, attributing this to the instability of subsurface oxides under negative cathodic potentials.[55] Additionally, the active site of Cu nanoparticles (NPs) is reported to be metallic Cu nanograin, as investigated through the structural dynamics during the life cycle of Cu NPs using liquid cell scanning transmission electron microscopy.[56] Therefore, the real active sites and structural evolution of OD-Cu under eCO_2RR reaction conditions remain unclear.

2.3. Grain boundaries

Grain boundaries (GBs), as structural defects, can create significant structural perturbations in their vicinity, inducing dislocations in the GBs region and leading to lattice strains (either compressive or tensile strains). In other words, GBs can generate high-energy surfaces through stabilized dislocations, which are thermodynamically favorable for catalysis.[57] To enhance the selectivity for multi-carbon products, various strategies have been developed to engineer GBs structures. These structures can adjust the adsorption energy of key intermediates on the catalyst surface, thus enhancing product selectivity.[58,59] For example, Chen *et al.* used PVP as an additive to control the growth rate of Cu during electrodeposition, resulting in Cu with abundant GBs (Fig. 4a). This catalyst achieves 70% selectivity for ethylene and ethanol across a wide potential range.[26] Han and colleagues found that the oxide/hydroxide crystals in HQ-Cu (containing Cu, Cu_2O, CuO) and AN-Cu (containing Cu, $Cu(OH)_2$) fragment into nanosized irregular Cu grains under applied cathodic potentials (Fig. 4b). This fragmentation results from oxidation–reduction cycling, which not only creates a complex GBs network but also exposes various high-index facets. These structural features facilitate C–C coupling, thereby enhancing the selectivity for C_{2+} products.[23] Huang *et al.* prepared La_2CuO_4 nanobamboo perovskites with abundant twin boundaries, achieving a 60% faradaic efficiency (FE) for ethylene. The high ethylene selectivity is attributed to the active (113) surface with inherent strain effects (Fig. 4c).[27] Therefore, designing and constructing unique GBs structures is highly beneficial for eCO_2RR reactions.

In complex GBs systems, single strategy often fails to meet practical needs in catalyst design. Combining multiple structural defects as active sites is often necessary to construct complex GBs structures, where various structural characteristics synergistically enhance the activity and stability of catalysts.[47,61,62] For OD-Cu, the active Cu^+ species inevitably undergoes electrochemical reduction to bulk metallic Cu at high current densities,[63] leading to poor selectivity for C_{2+} products. This presents a significant challenge for the effective utilization of OD-Cu. However, research indicates that abundant nanograin boundaries can enhance the stability of catalyst morphology and Cu^0/Cu^+ interfaces under high polarization and high current densities, preventing catalyst reconstruction and improving catalytic stability (Fig. 4d).[60] Moreover, nanograin boundaries and Cu^0/Cu^+ interfaces can increase *CO adsorption strength, promoting CO-CO coupling toward C_{2+} products.[56,64] Therefore, constructing intricate structures assembles with abundant nanograin boundaries and Cu^0/Cu^+ interfaces in Cu-based catalysts holds promise for achieving efficient eCO_2RR to C_{2+} products. Additionally, oxygen vacancies, a well-known defect, are widely employed to tailor the properties of catalysts.[2,65,66] For example, due to their

Open Access Article. Published on 23 June 2025. Downloaded on 4/15/2026 7:29:37 PM.
This article is licensed under a Creative Commons Attribution-NonCommercial 3.0 Unported Licence.

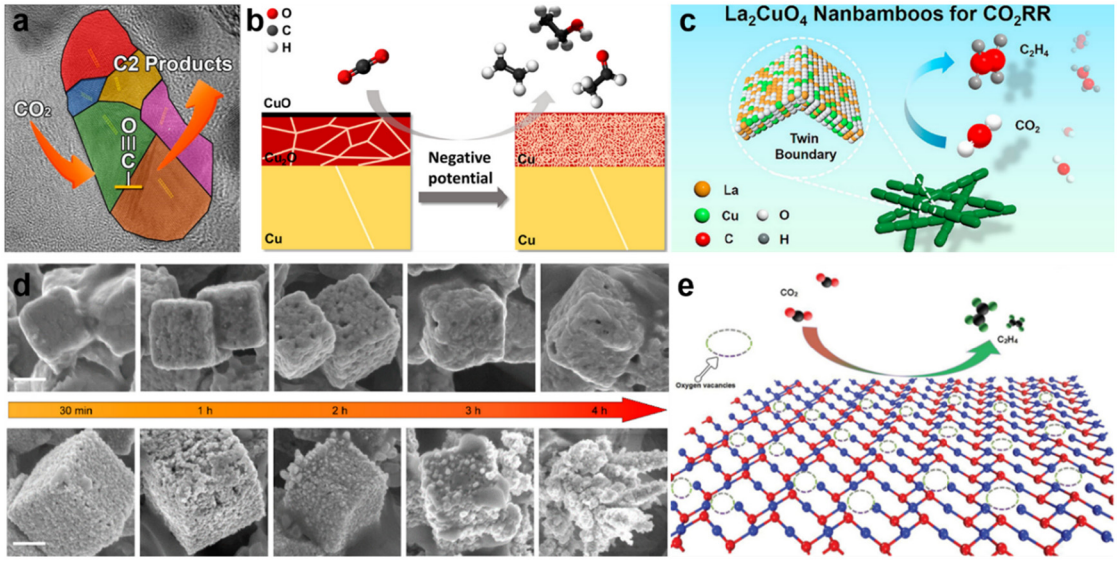

Fig. 4 Grain boundaries for eCO_2RR. (a) Illustration of the eCO_2RR process on the grain boundaries-rich Cu catalyst.[26] Reprinted with permission. Copyright 2020 American Chemical Society. (b) The fragmentation process of oxide/hydroxide crystals into nanosized irregular Cu grains under the applied negative potentials.[23] Reprinted with permission. Copyright 2020 American Chemical Society. (c) The La_2CuO_4 nanobamboo (La_2CuO_4 NBs) perovskite with rich twin boundaries showing a high FE of 60% toward ethylene.[27] Reprinted with permission. Copyright 2021 American Chemical Society. (d) SEM images of dynamic structure evolution for $Cu_2O(CO)$ and Cu_2O electrocatalysts during eCO_2RR.[60] Reprinted with permission. Copyright 2023 American Chemical Society. (e) Schematic of electrocatalytic reduction of CO_2 on Vo-rich CuO_x–Vo surface to C_2H_4.[61] Reprinted with permission. Copyright 2018 WILEY-VCH Verlag GmbH & Co. KGaA, Weinheim.

weakly bounded electrons, oxygen vacancies serve as excellent Lewis base sites to enhance the binding affinities of key intermediates (such as *CO and *COH), thereby promoting the production of C_2 (Fig. 4e).[61] Moreover, a higher concentration of oxygen vacancies near active sites is favorable for activating CO_2 molecules, lowering the reaction barrier for target products.[67] Therefore, integrating oxygen vacancies with grain boundaries and interface engineering is likely to modulate the surface electronic structure and concentration of active sites, thus accelerating reaction kinetics. However, effectively constructing oxygen vacancies and interface structures on catalyst surface remains highly challenging. Gaining a deeper understanding of the synergistic interactions between oxygen vacancies and interface structures will offer valuable guidance for the rational design of catalysts.

2.4. Morphology modification

The morphology of Cu nanostructures, such as size, shape, and crystal facets, significantly impacts the selectivity of eCO_2RR towards multi-carbon products.[28,68,69] The Cu(100) facet favors ethylene production, whereas the Cu(111) facet promotes methane production.[69] Buonsanti *et al.* synthesized Cu nanocrystals with varying sizes and shapes using a consistent colloidal method. The results demonstrated that cubic Cu nanocrystals exhibit higher ethylene selectivity than spherical ones, primarily due to the dominant presence of the Cu(100) facet.[28] Among the cubic Cu nanocrystals, those with a 44 nm edge length exhibit the highest eCO_2RR activity and ethylene selectivity compared to cubes with edge lengths of 24 nm and 63 nm, revealing a non-monotonic size-dependent selectivity in cubic Cu nanocrystals (Fig. 5a).[28] Mild plasma treatment introduces oxygen/chlorine ions into Cu nanocubes, the surface and subsurface oxygen species could influence the binding strength of CO on the surface, promoting the formation of multi-carbon products such as ethylene, ethanol, and isopropanol.[70] Song *et al.* reported that branched CuO nanoparticles achieve over 70% ethylene selectivity after activation. Compared to the cubic morphology, the initial branched CuO structure forms highly active interfaces and junctions in-between during activation, resulting in a large surface area and high local pH (Fig. 5b).[71] Yang and colleagues demonstrated that densely packed Cu NPs, after undergoing structural rearrangement during the eCO_2RR reaction, transform into a mixture of highly active cubic particles and smaller nanoparticles. At lower overpotentials (−0.53 V *vs.* RHE), selective formation of C_2–C_3 products can be achieved.[72]

Additionally, when high-curvature structures such as nanoneedles and nanodendrites are involved, they significantly impacts the catalyst's structure and catalytic mechanism.[74] For instance, nanoneedles can promote the nucleation of smaller gas bubble,[75] facilitating field-induced reactant concentration.[76,77] The high local electric field can cause the accumulation of charged cations, stabilizing reaction intermediates and enhancing eCO_2RR activity.[78] Edward *et al.* reported that the morphology of Cu derived from a sol–gel is controlled by electro-redeposition. Depending on the applied potentials, different structural morphologies, including nanoclusters, nanoneedles, nanowhiskers, and nanodendrites, appear sequentially (Fig. 5c). This growth results from the simultaneous dissolution and redeposition process of Cu ions from the bulk phase.[47] Inspired by gas-trapping phenomenon observed in spiders, hier-

 This journal is © The Royal Society of Chemistry 2025

Open Access Article. Published on 23 June 2025. Downloaded on 4/15/2026 7:29:37 PM.
This article is licensed under a Creative Commons Attribution-NonCommercial 3.0 Unported Licence.

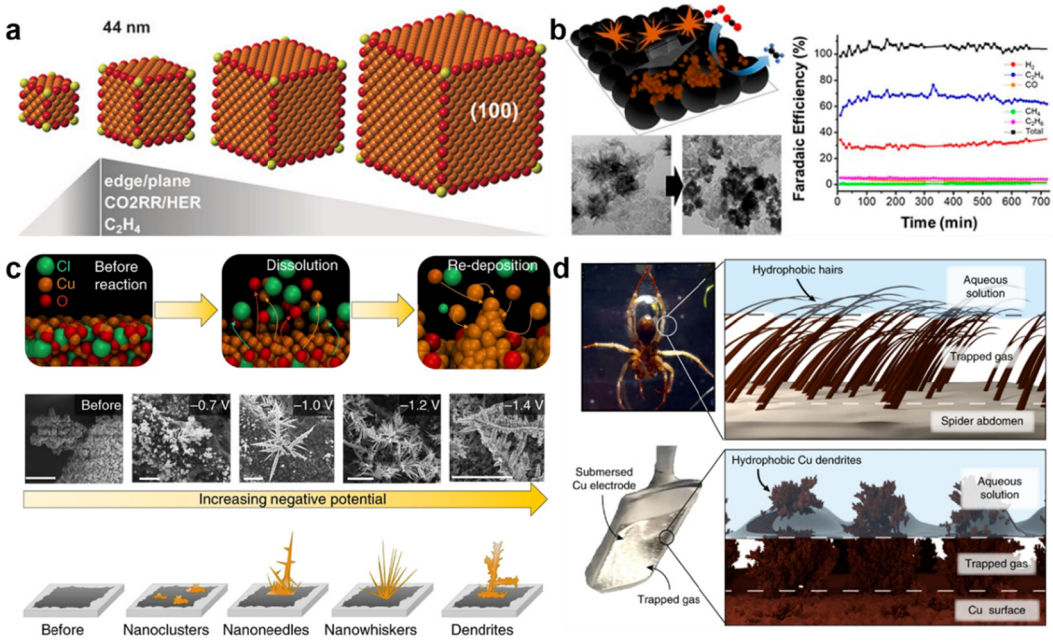

Fig. 5 Morphology effect for eCO_2RR. (a) Schematic of a non-monotonic size-dependence of the selectivity in cube-shaped copper nanocrystals.[28] Reprinted with permission. Copyright 2016 WILEY-VCH Verlag GmbH & Co. KGaA, Weinheim. (b) Schematic illustrating the transformation process of branched CuO NPs on conductive carbon materials during activation.[71] Reprinted with permission. Copyright 2019 American Chemical Society. (c) Schematic of the electro-growth process, whereby simultaneous dissolution and redeposition of Cu results in structured deposits.[47] Reprinted with permission. Copyright 2018 Springer Nature. (d) The plastron effect: the use of a hydrophobic surface to trap a layer of gas between the solution–solid interface. This is illustrated on a diving bell spider for subaquatic breathing and on a hydrophobic dendritic Cu surface for aqueous CO_2 reduction.[73] Reprinted with permission. Copyright 2019 Springer Nature.

archically structured Cu dendrites undergo surface hydrophobic treatment with 1-octadecanethiol. The treated electrodes can capture CO_2 gas at the electrolyte-electrode interface, forming a triple-phase boundary (Fig. 5d), which effectively suppresses HER and promotes eCO_2RR reactions.[73] In summary, the morphology effect offers a promising paradigm for the design and development of Cu-based electrocatalysts.

3. The CO_2 electrolyzer

There are three main configurations for CO_2 electrolyzers: H-cells, flow cell, and membrane electrode assembly (MEA).

3.1. H-cells

Most initial performance evaluations of eCO_2RR and catalyst screening are typically conducted using an H-cell. This system involves three electrodes: the working electrode and reference electrode are placed in the cathode chamber, while the counter electrode is fixed in the anode chamber. The cathode and anode chambers are separated by an ion-exchange membrane (Fig. 6).[79,80] This simple setup facilitates rapid catalyst screening. CO_2 is bubbled into the cathode chamber to maintain a CO_2-saturated electrolyte. Although some eCO_2RR catalysts have shown excellent performance in H-cells (Table 1), their practical application is constrained by several factors. The CO_2 concentration near the catalyst is limited by its solubility (approximately 34 mM at room temperature), resulting in mass transport constraints, which cap the maximum operating current at below 100 mA cm^{-2}.[81,82] eCO_2RR performance testing is typically conducted under neutral conditions to

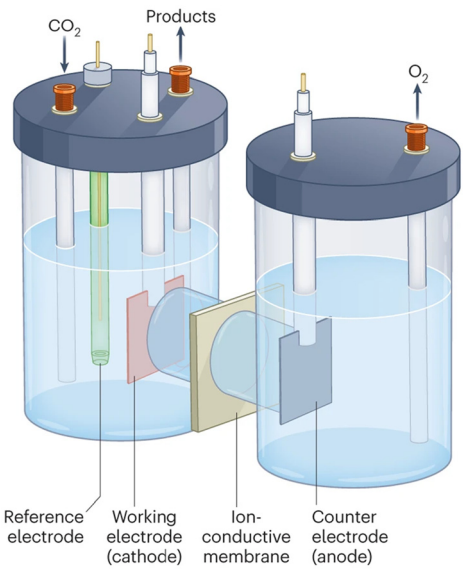

Fig. 6 Schematic illustration of three-electrode H-cells.[80] Reprinted with permission. Copyright 2023 Springer Nature.

Open Access Article. Published on 23 June 2025. Downloaded on 4/15/2026 7:29:37 PM. This article is licensed under a Creative Commons Attribution-NonCommercial 3.0 Unported Licence.

Table 1 The reported performance of eCO_2RR in different CO_2 electrolyzer

Electrolyzer	Catalyst	Electrolyte	V (*vs.* RHE/full-cell voltage)	Total current density (mA cm^{-2})	Stability (h)	Main product (FE)	Ref.
H-cell	Cu NPs	0.1 M $KHCO_3$	1.7 *vs.* Ag/AgCl	7.5	—	C_2H_4 (92.8%)	99
	Carbon-supported Cu	0.1 M $KHCO_3$	−0.6 V_{RHE}	1.5	16	Ethanol (91%)	100
	Cu NPs	0.1 M $KHCO_3$	−0.81 V_{RHE}	12.8	—	*n*-Propanol (5.9%)	72
	Nitrogen-doped nanodiamond	0.5 M $NaHCO_3$	−0.8 to −0.1 V_{RHE}	~7	3	Acetate (77%)	101
	Sn coupled with defective CuO	[Bmim]BF_4/H_2O	−2.0 V *vs.* Ag/Ag^+	67	36	Methanol (88.6%)	102
	CuAg	0.1 M $KHCO_3$	−1.1 V_{RHE}	40	17	CH_4 (50%)	22
	Ni/Fe-NC	0.5 M $KHCO_3$	−0.7 V_{RHE}	9.5	>30	CO (98%)	103
	3D core–shell porous-structured Cu@Sn	0.5 M $KHCO_3$	−0.93 V_{RHE}	16.52	15	Formate (100%)	104
Flow cell	DVL-Cu@GDL	0.5 M KCl	—	150	55	C_2H_4 (74%)	105
	Graphite/carbon NPs/Cu	7 M KOH	0.55 V_{RHE}	55–70	150	C_2H_4 (70%)	93
	Cu/Cu_2O	1 M KOH	−0.66 V_{RHE}	200	50	Ethanol (56%)	106
	CuAl2O4/CuO	1 M KOH	—	200	150	Ethanol (41%)	107
	b-Cu_2O/Cu	1 M KOH	−1.3 V_{RHE}	1000	16	*n*-Propanol (7.1%)	108
	Hg-CoTPP with N-doped graphene	1 M KOH	−0.8 V_{RHE}	420	360	CO (~100%)	109
	Grain boundary-enriched bismuth	1 M $KHCO_3$	−0.77 V_{RHE}	450	—	Formate (97%)	110
	$CuGa_2$	1 M KOH	−0.3 V_{RHE}	21.4	24	Methanol (78%)	111
	$Cu_1Sm\text{-}O_x$	1 M KOH	−1.35 V_{RHE}	500	24	CH_4 (65%)	112
	$CuGaO_2$ nanosheet	1 M KOH	−2 V_{RHE}	1000	5	CH_4 (68–55%)	113
MEA	F–Cu	0.1 M $KHCO_3$	−3.7	316	35	C_2H_4 (55.6%)	114
	CuO nanoplate	0.5 M $KHCO_3$	−3.2	200	—	C_2H_4 (80%)	105
	Cu_3Sn	1 M KOH	−3	900	48	Ethanol (40%)	115
	Copper(II) phthalocyanine	0.05 M $KHCO_3$	−4.2	190	110	CH_4 (56%)	116
	Cu nanoparticles supported on N-doped carbon	0.1 M $KHCO_3$	−4	230	50	CH_4 (60%)	117
	Ni-NCB	0.1 M $KHCO_3$	−2.8V	8300	6	CO (90%)	118
	Porous Ag	0.1 M $KHCO_3$	—	500	25	CO (74%)	119

avoid side reactions, such as carbonate formation in alkaline electrolytes and HER in acidic electrolytes.[80] However, the eCO_2RR reaction and pathways are highly dependent on the local reaction microenvironment, which influences the reaction energetics on the catalyst surface.[79,83] Consequently, catalysts developed in H-cells may perform significantly differently under industrial conditions due to variations in reaction microenvironments. Furthermore, impurities deposition on the catalyst surface can affect the eCO_2RR reaction pathways, leading to catalyst deactivation.[84,85] Therefore, alternative testing systems are needed to evaluate the catalyst performance under industrially relevant eCO_2RR conditions.

3.2. Flow cells

To address the challenges of low CO_2 solubility, low current density, and mass transport limitations in H-cells, gas diffusion electrodes (GDEs) have been developed. GDEs significantly shorten the diffusion path of CO_2 to the electrode surface (approximately 50 nm), enhancing mass transport efficiency and enabling the industrial application of eCO_2RR.[83,86] Unlike H-cells, flow cells can effectively utilize alkaline electrolytes, which are unsuitable for H-cells. GDEs allow separation of the CO_2 flow field from the liquid electrolytes, maintaining a high local pH on the catalyst surface, which inhibits HER and promotes C–C coupling.[87–89] This configuration allows for high product selectivity at high current densities, positioning flow cells as a potential replacement for H-cells in eCO_2RR performance testing. In the flow cell configuration (Fig. 7a), the catholyte and anolyte circulate through the cathode and anode chambers, respectively. The cathode and anode chambers are separated by an ion exchange membrane. Gaseous CO_2 is continuously supplied to the cathode catalyst.[90,91]

Current research on eCO_2RR catalysts has transitioned from H-cells to flow cells. The complexity of flow cell configurations has driven the evolution of catalyst material design into a multifaceted approach, encompassing the catalyst, the local microenvironment, and the overall system (Table 1). The catholyte can regulate the local microenvironment on the catalyst surface, optimizing CO_2 conversion efficiency (Fig. 7b). For example, Dinh *et al.* showed that a high concentration of KOH electrolyte can significantly reduce the onset potential for eCO_2RR.[93] Chen and colleagues reported that Cu-polyamine in a strong alkaline electrolyte (10 M KOH) can achieve an 87% FE for ethylene.[87] Elevated pH levels can reduce H coverage on the catalyst surface, thus inhibiting HER. This enhanced catalytic activity can, in turn, lower the cell voltage, thereby improving energy efficiency (Fig. 7c). Although strong alkaline electrolytes can accelerate the formation of multi-carbon products,[93]

 This journal is © The Royal Society of Chemistry 2025

Open Access Article. Published on 23 June 2025. Downloaded on 4/15/2026 7:29:37 PM.
This article is licensed under a Creative Commons Attribution-NonCommercial 3.0 Unported Licence.

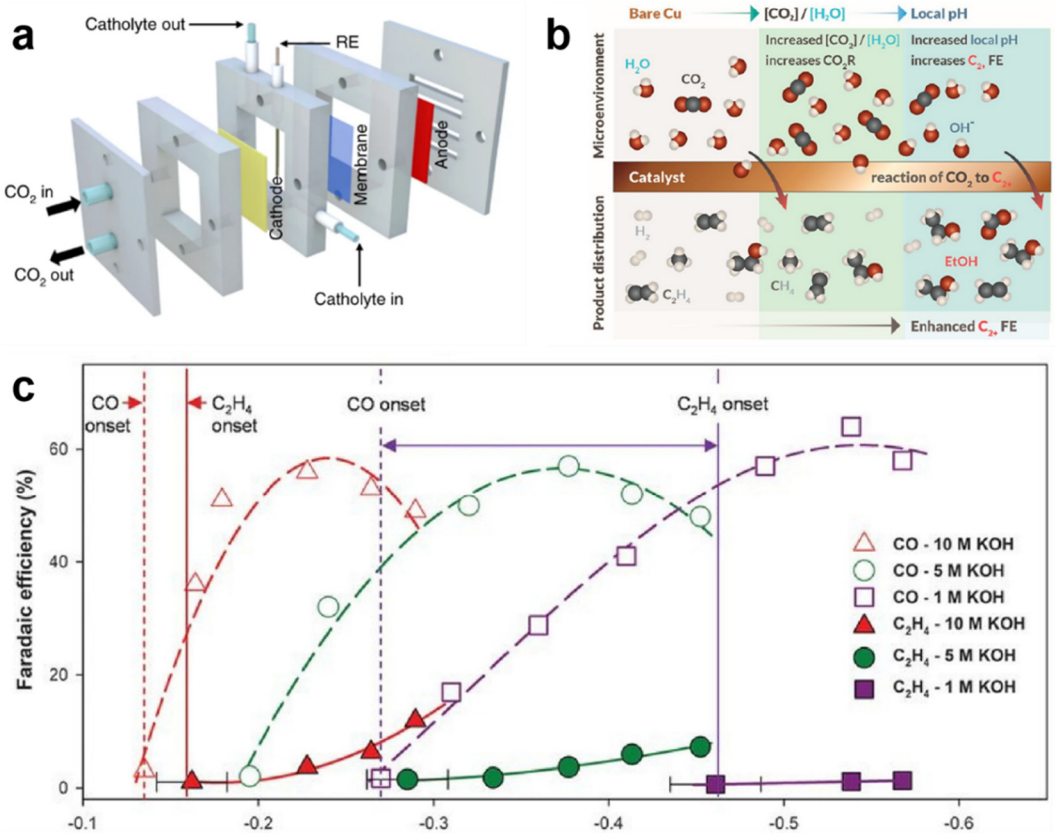

Fig. 7 (a) Schematic illustration of flow cells.[91] Reprinted with permission. Copyright 2019 Springer Nature. (b) Schematic illustration of the local microenvironment and its effect on eCO_2RR selectivity.[92] Reprinted with permission. Copyright 2022 American Chemical Society. (c) C_2H_4 and CO FEs showing the reduction of C_2H_4 onset potential with increasing KOH concentrations.[93] Reprinted with permission. Copyright 2018 The American Association for the Advancement of Science.

they also lead to low CO_2 utilization efficiency and irreversible electrolyte acidification,[94,95] creating challenges for optimal performance. In acidic electrolytes, the FE of HER side reaction is typically 20% or higher, making it energy-intensive and inhibitory to the eCO_2RR reaction.[96] To address these issues, neutral electrolytes like potassium bicarbonate have been employed, though product selectivity of eCO_2RR in neutral electrolyte is lower than in alkaline environments.[97,98] Overall, the flow cell configurations overcome the limitations of H-cells, facilitating the large-scale application of eCO_2RR.

3.3. MEA electrolyzer

In a flow cell, liquid electrolytes in the cathode and anode chambers create high resistance, lowering the overall energy efficiency of the system. To tackle this issue, a practical approach is to remove the liquid electrolyte between the electrodes, leading to the development of the membrane electrode assembly (MEA).[120] An MEA operates as a dual-electrode zero-gap cell, with a polymer electrolyte membrane sandwiched between the anode and cathode. The electrolyte circulates through the porous anode without the need for a reference electrode. Humidified CO_2 is continuously supplied to the cathode's GDE (Fig. 8a). Compared to flow cells, the MEA configuration leverages the gas diffusion electrode (GDE) of a flow cell, minimizing the electrolyte usage by enabling direct contact between the catalyst layer and the ion exchange membrane. This design mitigates cell resistance, boosts energy efficiency, and enhances cell stability, making it more feasible for practical applications.[95]

The formation of multi-carbon products in an MEA electrolyzer has yet to be extensively studied (Table 1). Gabardo *et al.* demonstrate the potential for multi-carbon product formation in an MEA reactor by sputtering Cu onto a porous PTFE membrane as the catalyst and adjusting the reaction temperature to 40 °C, achieving 30% ethylene selectivity.[121] Gong *et al.* reported that oxygen-rich ultrathin CuO nanoplate arrays could achieve 80% ethylene selectivity at a current density of 200 mA cm^{-2} (Fig. 8b). Compact evaporated Cu films and stable nanostructures effectively prevent GDL flooding during eCO_2RR testing, enhancing the long-term stability of the catalyst.[105] Zheng *et al.* reported that a low-entropy Cu_3Sn catalyst maintains stability for over 48 h at industrial-scale current densities, with 40% ethanol selectivity (Fig. 8c).[115] Gu *et al.* constructed a defect-rich surface by electrodepositing Cu in a CO-rich atmosphere, significantly promoting CO_2 conversion to ethanol, achieving 70% FE for C_{2+} alcohols at a partial current density of 100 mA cm^{-2}. In a 30 h stability test, the MEA electrolyzer produces 500 mg of C_{2+} alcohols per cm^2 of catalyst (Fig. 8d).[122] In summary, MEA electrolyzers may offer better

Open Access Article. Published on 23 June 2025. Downloaded on 4/15/2026 7:29:37 PM.
This article is licensed under a Creative Commons Attribution-NonCommercial 3.0 Unported Licence.

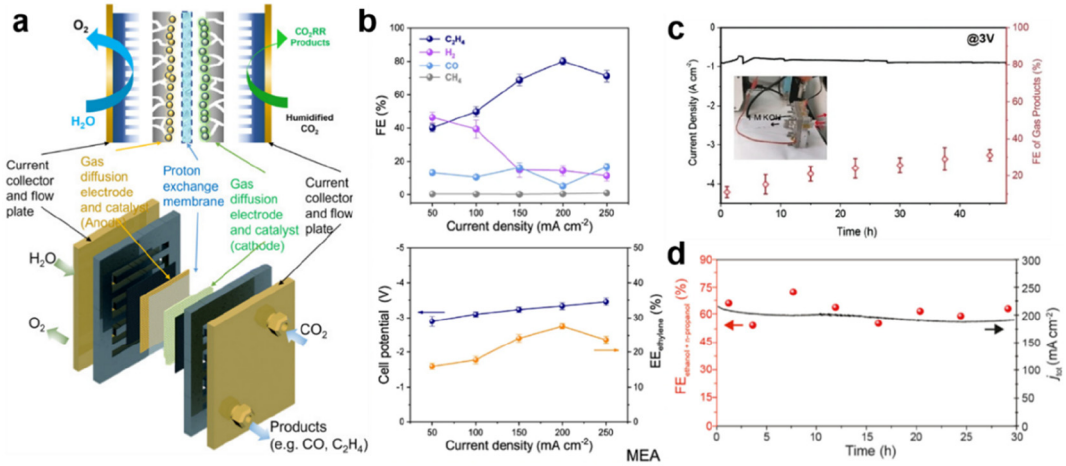

Fig. 8 (a) Schematic of membrane-electrode assembly for eCO_2RR.[120] Reprinted with permission. Copyright 2022 Elsevier. (b) Gas product FEs, cell potential and energy efficiency for C_2H_4 of the DVL-Cu@GDL catalyst in an MEA electrolyzer.[105] Reprinted with permission. Copyright 2022 Springer Nature. (c) The long-term stability test of Cu_3Sn in 1 M KOH at 3 V.[115] Reprinted with permission. Copyright 2021 WILEY-VCH Verlag GmbH & Co. KGaA, Weinheim. (d) eCO_2RR to ethanol using Cu-DS catalyst in a MEA system during 30 h of electrolysis under a full-cell voltage of 3.5 V.[122] Reprinted with permission. Copyright 2021 Elsevier.

stability than flow cells and H-cells, making them more attractive for commercial applications.

4. Mechanistic insights

In-depth investigation of the reaction mechanism is crucial for the rational design of Cu-based electrocatalysts. By elucidating the nature and dynamic evolution of active sites during the eCO_2RR reaction, mechanistic insights can provide a theoretical foundation for the functional design of catalysts, thereby avoiding inefficient and blind screening processes and enabling the precise development of high-performance catalytic materials. Currently, most mechanistic studies of eCO_2RR rely on *ex situ* characterization methods.[25,41,123] However, under practical eCO_2RR conditions, the structure and active sites of catalysts can undergo significant dynamic transformations.[124] For instance, in Cu-based catalysts, it has been traditionally believed that oxidative $Cu^{\delta+}$ species are inevitably reduced to metallic Cu under cathodic potentials, making metallic Cu widely regarded as the dominant active phase.[114] Nevertheless, recent *in situ* Raman spectra studies have revealed the presence of oxidative $Cu^{\delta+}$ species, such as Cu_2O and Cu–OH species, even under strongly reducing conditions.[114,124] These species can originate not only from the precursor but also form dynamically on the surface of metallic Cu NPs during eCO_2RR conditions. Moreover, theoretical calculations have shown that oxidative $Cu^{\delta+}$ species can promote C–C coupling more effectively, thus favoring the formation of C_{2+} products.[47,124] This suggests that metallic Cu is not the sole active site, and oxidative $Cu^{\delta+}$ species may play a more critical role under practical eCO_2RR conditions.

Most mechanistic studies to date have been conducted at low current densities, whereas industrial eCO_2RR systems typically operate at high current densities (>200 mA cm^{-2}).[74,94] Under such industrially relevant conditions, the stability and behavior of oxidative $Cu^{\delta+}$ species remain ambiguous. On one hand, conventional *in situ* electrochemical cells often suffer from high internal resistance, limiting their capacity to sustain high current operation.[114] On the other hand, extensive gas evolution at high current densities interferes with signal acquisition, preventing accurate detection of transient active species. Furthermore, these cells do not realistically simulate the operating environment of practical CO_2 electrolyzers. Changes in any component, such as electrolyte composition, catalyst layer structure, membrane type, or gas–liquid–solid triple-phase boundaries, can significantly affect eCO_2RR performance, complicating mechanistic interpretation.[125] To better mimic industrial conditions, it is imperative to develop *in situ*-compatible electrolyzer systems capable of operating at high current densities. Given that MEA-based electrolyzers are widely used in practical applications, *in situ* characterizations in MEA reactors have emerged as a promising platform for studying the dynamic evolution of catalysts under realistic operating conditions. However, due to the close contact between the catalyst layer and the membrane, Raman spectroscopy often fails to capture useful signals. In this context, *in situ* X-ray absorption spectroscopy (XAS), with its element-specific sensitivity and ability to resolve atomic-scale structural changes, presents a powerful alternative. XAS enables real-time tracking of catalyst structural evolution under operational conditions, paving the way for deeper mechanistic understanding and the targeted design of advanced eCO_2RR catalysts.

5. System optimization in eCO_2RR

5.1. Electrolyte engineering

The choice of electrolyte plays a fundamental role in dictating CO_2 solubility, proton availability, and the stabilization of key

 This journal is © The Royal Society of Chemistry 2025

Open Access Article. Published on 23 June 2025. Downloaded on 4/15/2026 7:29:37 PM. This article is licensed under a Creative Commons Attribution-NonCommercial 3.0 Unported Licence.

reaction intermediates. Optimizing the electrolyte composition is crucial for achieving high faradaic efficiency (FE) towards C_{2+} products while minimizing side reactions such as the HER. Electrolyte pH strongly influences the reaction pathway of CO_2 electroreduction. A neutral or slightly alkaline pH is often preferred because it maintains sufficient CO_2 availability while suppressing excessive HER. For example, potassium bicarbonate ($KHCO_3$) is a commonly used neutral electrolyte that ensures moderate proton availability and stable catalyst performance. Conversely, strongly alkaline electrolytes (*e.g.*, KOH) accelerate CO_2 depletion near the electrode due to rapid carbonate formation, which reduces eCO_2RR efficiency.[37] Bipolar membranes (BPMs) have been extensively studied as a means to decouple the pH at the cathode and anode, thereby optimizing reaction conditions for both CO_2 reduction and oxygen evolution. BPMs generate local proton gradients, which can facilitate selective eCO_2RR to C_{2+} products by stabilizing key intermediates such as CO dimer species. Studies have shown that BPM-integrated systems can significantly enhance ethylene and ethanol production rates while preventing catalyst degradation.[126] Adding alkali metal cations (*e.g.*, K^+, Cs^+, or Rb^+) to the electrolyte has been found to enhance C_{2+} selectivity. These cations interact with adsorbed CO intermediates, stabilizing them and promoting C–C coupling.[127]

Thus, electrolyte optimization remains a powerful approach for enhancing C_{2+} product formation in eCO_2RR, ensuring high selectivity while mitigating competing side reactions.

5.2. Gas diffusion electrodes

In an H-cell, the catalyst is typically deposited on a substrate such as carbon paper, glassy carbon rods, or directly on a metal foil as the working electrode. In aqueous electrolytes, this setup leads to sluggish mass transfer and low eCO_2RR reaction rates.[128,129] To enhance eCO_2RR performance, GDEs have been introduced, enabling CO_2 to diffuse directly to the electrode–electrolyte interface.[130] GDEs typically consist of a gas diffusion layer (GDL) and a catalyst layer (Fig. 9a).[93,131] This structure forms a three-phase interface where the liquid electrolyte and gaseous CO_2 coexist in the catalyst layer.[130] The GDL contains a dense carbonaceous network that serves as a porous support for the catalyst layer. This dense network, typically made from carbon fibers like carbon paper or PTFE, ensures mechanical stability and facilitates efficient gas transport. The dense carbon network in the GDL plays a crucial role in forming a stable and efficient interface for the electrochemical reactions in eCO_2RR systems.[132] The GDLs are typically treated with PTFE to enhance hydrophobicity, effectively preventing water infiltration. The nanoporous structure of the GDL ensures the transport of CO_2 gas to the catalyst layer. Maintaining GDE hydrophobicity is crucial during the eCO_2RR reaction.[133,134] Loss of hydrophobicity can cause electrolyte permeation into GDL pores, leading to flooding within the GDL. This obstructs CO_2 diffusion, inhibiting eCO_2RR and promoting HER.[135,136] Therefore, GDE stability is critical for long-term stability testing of CO_2 electrolyzers.

To overcome these challenges, researchers have incorporated hydrophobic PTFE frameworks into GDEs. Compared to carbon paper-based GDEs, hydrophobic PTFE exhibits better long-term stability during eCO_2RR testing. Sargent *et al.* sputtered Cu NPs onto porous PTFE and coated the catalyst surface with carbon nanoparticles and graphene to enhance conductivity, thereby creating a stable electrode interface (Fig. 9b). This setup achieved 70% ethylene selectivity at current den-

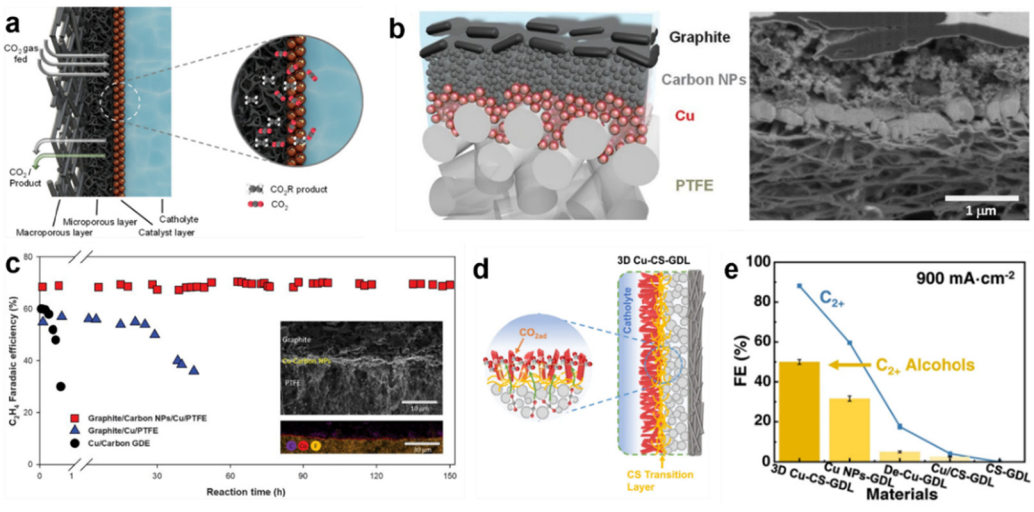

Fig. 9 (a) Schematic of an eCO_2RR GDE cathode and its fundamental components.[10] Reprinted with permission. Copyright 2024 American Chemical Society. (b) Structure of the polymer-based gas diffusion electrode.[93] Reprinted with permission. Copyright 2018 The American Association for the Advancement of Science. (c) The long-term stability test of polymer-based gas diffusion electrode.[93] Reprinted with permission. Copyright 2018 The American Association for the Advancement of Science. (d) Schematic of 3D Cu-CS-GDL electrode.[137] Reprinted with permission. Copyright 2023 Springer Nature. (e) The FE of C_{2+} products and C_{2+} alcohols on different GDEs at a current density of 900 mA cm^{-2}.[137] Reprinted with permission. Copyright 2023 Springer Nature.

Open Access Article. Published on 23 June 2025. Downloaded on 4/15/2026 7:29:37 PM. This article is licensed under a Creative Commons Attribution-NonCommercial 3.0 Unported Licence.

sities of 75 to 100 mA cm^{-2} in 7 M KOH electrolyte, with extended long-term stability testing up to 150 h without decay —300 times longer than traditional GDEs (Fig. 9c).[93] This GDE design has demonstrated structural superiority. Additionally, Han *et al.* coupled GDEs with 3D nanostructured catalysts to design a 3D Cu-chitosan (CS)-GDL electrode. CS acts as a transition layer between the Cu catalyst and the GDL (Fig. 9d). The highly interlaced network promotes the growth of 3D Cu films, facilitating rapid electron transfer and reducing mass transfer limitations. This structure achieved 88.2% C_{2+} selectivity at a current density of 900 mA cm^{-2} (Fig. 9e).[137] These advancements in GDE design underscore the importance of creating a stable and efficient interface for electrochemical reactions, highlighting the critical role of dense carbonaceous networks and hydrophobic treatments in achieving high performance and long-term stability in eCO_2RR systems.

6. Conclusion and outlook

In summary, eCO_2RR represents a key pathway for sustainable carbon management, and ongoing research is focused on overcoming the challenges of catalyst design, system optimization, and product selectivity. Further advancements in understanding reaction mechanisms, developing efficient catalysts, and optimizing system configurations are essential to enable large-scale deployment of eCO_2RR technology for the production of high-value chemicals and fuels.

Despite extensive efforts in eCO_2RR systems, several issues remain that must be addressed before commercialization. These issues primarily revolve product selectivity, stability, understanding of reaction mechanisms, and energy efficiency. The specific details are as follows:

(1) While C_1 products like CO and formate can achieve nearly 100% selectivity at high current densities, the selectivity for multi-carbon products remains insufficient for industrial applications. Although multi-carbon products could ideally serve as direct fuels, their high separation costs and the mixture of various gaseous and liquid products make them impractical for continuous supply in downstream reactions. Future efforts should focus on designing catalysts that improve the selectivity for single products, making them more practical for industrial applications.

(2) Industrial-scale eCO_2RR technology demands long-term stability. Challenges such as catalyst deactivation and the electrowetting effect of the GDL hinder the advancement of eCO_2RR technology. Therefore, ensuring the long-term operation of Cu-based catalysts in reactors remains a significant challenge. Anchoring catalysts onto superhydrophobic and highly stable GDLs could improve the stability of CO_2 electrolyzers.

(3) Previous mechanistic studies have generally concentrated on H-cell setups at the lab scale, which may not be applicable to flow cells and MEA reactors. The significant differences in current densities and configurations between flow cells, MEA reactors, and H-cells indicate that conventional *in situ* reaction cells may not accurately reflect the reaction processes in flow cells and MEAs. Therefore, developing appropriate *in situ* flow cell and MEA systems is essential for elucidating the true reaction mechanisms under realistic eCO_2RR conditions.

(4) In terms of electrolyzer design, conventional flow cells suffer from high internal resistance, resulting in elevated energy consumption and limiting their suitability for industrial-scale applications. As a result, research should shift toward the structural optimization of MEA electrolyzers. Although MEA systems offer advantages such as lower cell resistance, and higher energy efficiency, they face challenges in long-term stability. One of the major issues is membrane degradation, which leads to increased cell resistance, localized overheating, and diminished catalytic activity. Therefore, the development of highly durable membrane materials is essential for advancing the practical application of MEA systems. In addition, operational parameters within MEA systems, such as temperature and pressure, significantly influence overall performance. Introducing elevated temperature and pressure conditions can accelerate reaction kinetics and enhance catalytic activity. Lastly, given that the energy efficiency of current MEA electrolyzers typically remains below 50%, future studies should focus on strategies to reduce the overall cell voltage and improve C_{2+} product selectivity, thereby enhancing the energy efficiency of the system.

Although significant progress has been made, addressing these key issues is crucial for the commercial viability of eCO_2RR technologies. Focusing on these areas will facilitate the transition of eCO_2RR from laboratory research to large-scale industrial applications.

Author contributions

Yimin Wu conceived and supervised the project. L. W. and Y. A. W. wrote the manuscript. All authors made comments and revised the manuscript.

Conflicts of interest

The authors declare no competing interests.

Data availablity

No primary research results, software or code have been included.

Acknowledgements

Y. A. W. thanks the funding from New Frontiers Research Fund-Transformation (NFRFT-2022-00197), the Natural Sciences and Engineering Research Council of Canada (NSERC) (RGPIN-2020-05903, GECR-2020-00476), Tang Family

 This journal is © The Royal Society of Chemistry 2025

Open Access Article. Published on 23 June 2025. Downloaded on 4/15/2026 7:29:37 PM. This article is licensed under a Creative Commons Attribution-NonCommercial 3.0 Unported Licence.

Chair in New Energy Materials and Sustainability, Canadian Foundation for Innovation John R. Evans Leaders Fund (#41779), and Ontario Research Fund for Small Infrastructure (#41779).

References

1 W. Ye, X. Guo and T. Ma, A review on electrochemical synthesized copper-based catalysts for electrochemical reduction of CO_2 to C_{2+} products, *Chem. Eng. J.*, 2021, **414**, 128825.
2 X. Li, *et al.*, Strategies for enhancing electrochemical CO_2 reduction to multi-carbon fuels on copper, *Innovation Mater.*, 2023, **1**(1), 100014.
3 L. J. Nunes, The rising threat of atmospheric CO_2: a review on the causes, impacts, and mitigation strategies, *Environments*, 2023, **10**, 66.
4 O. S. Bushuyev, *et al.*, What should we make with CO_2 and how can we make it?, *Joule*, 2018, **2**, 825–832.
5 M. Chen, *et al.*, Advanced characterization enables a new era of efficient carbon dots electrocatalytic reduction, *Coord. Chem. Rev.*, 2025, **535**, 216612.
6 S. Gao, *et al.*, Isolated FeN_3 sites anchored hierarchical porous carbon nanoboxes for hydrazine–assisted rechargeable Zn–CO_2 batteries with ultralow charge voltage, *Carbon Energy*, 2025, **7**, e637.
7 L. Fan, *et al.*, Selective production of ethylene glycol at high rate via cascade catalysis, *Nat. Catal.*, 2023, **6**, 585–595.
8 Q. Lu and F. J. N. E. Jiao, Electrochemical CO_2 reduction: Electrocatalyst, reaction mechanism, and process engineering, *Nano Energy*, 2016, **29**, 439–456.
9 E. E. Benson, C. P. Kubiak, A. J. Sathrum and J. M. Smieja, Electrocatalytic and homogeneous approaches to conversion of CO_2 to liquid fuels, *Chem. Soc. Rev.*, 2009, **38**, 89–99.
10 C. P. O'Brien, *et al.*, CO_2 Electrolyzers, *Chem. Rev.*, 2024, **124**(7), 3648–3693.
11 H. Yang, *et al.*, Potential-driven structural distortion in cobalt phthalocyanine for electrocatalytic CO_2/CO reduction towards methanol, *Nat. Commun.*, 2024, **15**, 7703.
12 W. Niu, *et al.*, High-efficiency C_3 electrosynthesis on a lattice-strain-stabilized nitrogen-doped Cu surface, *Nat. Commun.*, 2024, **15**, 7070.
13 B. S. Crandall, *et al.*, Kilowatt-scale tandem CO_2 electrolysis for enhanced acetate and ethylene production, *Nat. Chem. Eng.*, 2024, **1**, 421–429.
14 H. Dau, *et al.*, The mechanism of water oxidation: from electrolysis via homogeneous to biological catalysis, *ChemCatChem*, 2010, **2**, 724–761.
15 R. Kortlever, J. Shen, K. J. P. Schouten, F. Calle-Vallejo and M. T. Koper, Catalysts and reaction pathways for the electrochemical reduction of carbon dioxide, *J. Phys. Chem. Lett.*, 2015, **6**, 4073–4082.
16 Y.-J. Zhang, V. Sethuraman, R. Michalsky and A. A. Peterson, Competition between CO_2 reduction and H_2 evolution on transition-metal electrocatalysts, *ACS Catal.*, 2014, **4**, 3742–3748.
17 Y. i. Hori, Electrochemical CO_2 reduction on metal electrodes, *Mod. Aspects Electrochem.*, 2008, 89–189.
18 T. T. Hoang, *et al.*, Nanoporous copper–silver alloys by additive-controlled electrodeposition for the selective electroreduction of CO_2 to ethylene and ethanol, *J. Am. Chem. Soc.*, 2018, **140**, 5791–5797.
19 Z. Chang, S. Huo, W. Zhang, J. Fang and H. Wang, The tunable and highly selective reduction products on Ag@Cu bimetallic catalysts toward CO_2 electrochemical reduction reaction, *J. Phys. Chem. C*, 2017, **121**, 11368–11379.
20 L. Chen, *et al.*, Energy-efficient CO(2) conversion to multicarbon products at high rates on CuGa bimetallic catalyst, *Nat. Commun.*, 2024, **15**, 7053.
21 D. Wang, *et al.*, Revealing the structural evolution of CuAg composites during electrochemical carbon monoxide reduction, *Nat. Commun.*, 2024, **15**, 4692.
22 L. Wang, *et al.*, Enhanced CO_2-to-CH_4 conversion via grain boundary oxidation effect in CuAg systems, *Chem. Eng. J.*, 2024, **500**, 156728.
23 Q. Lei, *et al.*, Investigating the origin of enhanced C_{2+} selectivity in oxide-/hydroxide-derived copper electrodes during CO_2 electroreduction, *J. Am. Chem. Soc.*, 2020, **142**, 4213–4222.
24 S. Y. Lee, *et al.*, Mixed copper states in anodized Cu electrocatalyst for stable and selective ethylene production from CO_2 reduction, *J. Am. Chem. Soc.*, 2018, **140**, 8681–8689.
25 L. Chen, *et al.*, Additive-assisted electrodeposition of Cu on gas diffusion electrodes enables selective CO_2 reduction to multicarbon products, *ACS Catal.*, 2023, **13**, 11934–11944.
26 Z. Chen, *et al.*, Grain-boundary-rich copper for efficient solar-driven electrochemical CO_2 reduction to ethylene and ethanol, *J. Am. Chem. Soc.*, 2020, **142**, 6878–6883.
27 J. Wang, *et al.*, Grain-boundary-engineered La_2CuO_4 perovskite nanobamboos for efficient CO_2 reduction reaction, *Nano Lett.*, 2021, **21**, 980–987.
28 A. Loiudice, *et al.*, Tailoring copper nanocrystals towards C_2 products in electrochemical CO_2 reduction, *Angew. Chem., Int. Ed.*, 2016, **55**, 5789–5792.
29 M. Ma, K. Djanashvili and W. A. Smith, Controllable hydrocarbon formation from the electrochemical reduction of CO_2 over Cu nanowire arrays, *Angew. Chem., Int. Ed.*, 2016, **55**, 6680–6684.
30 M. Chen, *et al.*, Cutting-edge innovations in red carbon dots: Synthesis, perfection, and breakthroughs in optoelectronics and electrocatalysis, *Chem. Eng. J.*, 2024, 155302.
31 D. Xue, H. Xia, W. Yan, J. Zhang and S. Mu, Defect engineering on carbon-based catalysts for electrocatalytic CO_2 reduction, *Nano-Micro Lett.*, 2021, **13**, 1–23.

Open Access Article. Published on 23 June 2025. Downloaded on 4/15/2026 7:29:37 PM. This article is licensed under a Creative Commons Attribution-NonCommercial 3.0 Unported Licence.

32 M. Moura de Salles Pupo and R. Kortlever, Electrolyte effects on the electrochemical reduction of CO_2, *ChemPhysChem*, 2019, **20**, 2926–2935.
33 Y. Jia, F. Li, K. Fan and L. Sun, Cu-based bimetallic electrocatalysts for CO_2 reduction, *Adv. Powder Mater.*, 2022, **1**, 100012.
34 W. Zhu, *et al.*, Formation of enriched vacancies for enhanced CO_2 electrocatalytic reduction over AuCu alloys, *ACS Energy Lett.*, 2018, **3**, 2144–2149.
35 X. Zhang, X. Sun, S.-X. Guo, A. M. Bond and J. Zhang, Formation of lattice-dislocated bismuth nanowires on copper foam for enhanced electrocatalytic CO_2 reduction at low overpotential, *Energy Environ. Sci.*, 2019, **12**, 1334–1340.
36 W. Zhu, B. M. Tackett, J. G. Chen and F. Jiao, Bimetallic electrocatalysts for CO_2 reduction, *Electrocatalysis*, 2020, 105–125.
37 K. P. Kuhl, E. R. Cave, D. N. Abram and T. F. Jaramillo, New insights into the electrochemical reduction of carbon dioxide on metallic copper surfaces, *Energy Environ. Sci.*, 2012, **5**, 7050–7059.
38 H. Zhang, *et al.*, Computational and experimental demonstrations of one-pot tandem catalysis for electrochemical carbon dioxide reduction to methane, *Nat. Commun.*, 2019, **10**, 3340.
39 C.-J. Chang, *et al.*, Dynamic reoxidation/reduction-driven atomic interdiffusion for highly selective CO_2 reduction toward methane, *J. Am. Chem. Soc.*, 2020, **142**, 12119–12132.
40 W. J. Dong, *et al.*, Tailoring electronic structure of bifunctional Cu/Ag layered electrocatalysts for selective CO_2 reduction to CO and CH_4, *Nano Energy*, 2020, **78**, 105168.
41 C. Chen, *et al.*, Cu-Ag tandem catalysts for high-rate CO_2 electrolysis toward multicarbons, *Joule*, 2020, **4**, 1688–1699.
42 W. Fu, *et al.*, Preserving Molecular Tuning for Enhanced Electrocatalytic CO_2-to-Ethanol Conversion, *Angew. Chem.*, 2024, **136**, e202407992.
43 X. Lv, *et al.*, Electron–deficient Cu sites on Cu_3Ag_1 catalyst promoting CO_2 electroreduction to alcohols, *Adv. Energy Mater.*, 2020, **10**, 2001987.
44 S. Ma, *et al.*, Electroreduction of carbon dioxide to hydrocarbons using bimetallic Cu–Pd catalysts with different mixing patterns, *J. Am. Chem. Soc.*, 2017, **139**, 47–50.
45 C. G. Morales-Guio, *et al.*, Improved CO_2 reduction activity towards C_{2+} alcohols on a tandem gold on copper electrocatalyst, *Nat. Catal.*, 2018, **1**, 764–771.
46 H. Mistry, *et al.*, Highly selective plasma-activated copper catalysts for carbon dioxide reduction to ethylene, *Nat. Commun.*, 2016, **7**, 1–9.
47 P. De Luna, *et al.*, Catalyst electro-redeposition controls morphology and oxidation state for selective carbon dioxide reduction, *Nat. Catal.*, 2018, **1**, 103–110.
48 F. Dattila, R. García-Muelas and N. r. López, Active and selective ensembles in oxide-derived copper catalysts for CO_2 reduction, *ACS Energy Lett.*, 2020, **5**, 3176–3184.
49 M. Fang, *et al.*, Hydrophobic, ultrastable Cuδ+ for robust CO_2 electroreduction to C_2 products at ampere-current levels, *J. Am. Chem. Soc.*, 2023, **145**, 11323–11332.
50 Y. Zhou, *et al.*, Dopant-induced electron localization drives CO_2 reduction to C_2 hydrocarbons, *Nat. Chem.*, 2018, **10**, 974–980.
51 D. Ren, *et al.*, Selective electrochemical reduction of carbon dioxide to ethylene and ethanol on copper(I) oxide catalysts, *ACS Catal.*, 2015, **5**, 2814–2821.
52 L. Fan, Z. Xia, M. Xu, Y. Lu and Z. Li, 1D SnO_2 with Wire-in-Tube Architectures for Highly Selective Electrochemical Reduction of CO_2 to C_1 Products, *Adv. Funct. Mater.*, 2018, **28**, 1706289.
53 C. W. Li, J. Ciston and M. W. Kanan, Electroreduction of carbon monoxide to liquid fuel on oxide-derived nanocrystalline copper, *Nature*, 2014, **508**, 504–507.
54 Z.-Q. Liang, *et al.*, Copper-on-nitride enhances the stable electrosynthesis of multi-carbon products from CO_2, *Nat. Commun.*, 2018, **9**, 1–8.
55 Y. Lum and J. W. Ager, Stability of residual oxides in oxide–derived copper catalysts for electrochemical CO_2 reduction investigated with 18O labeling, *Angew. Chem., Int. Ed.*, 2018, **57**, 551–554.
56 Y. Yang, *et al.*, Operando studies reveal active Cu nanograins for CO_2 electroreduction, *Nature*, 2023, **614**, 262–269.
57 X. She, *et al.*, Grain-boundary surface terminations incorporating oxygen vacancies for selectively boosting CO_2 photoreduction activity, *Nano Energy*, 2021, **84**, 105869.
58 R. G. Mariano, K. McKelvey, H. S. White and M. W. Kanan, Selective increase in CO_2 electroreduction activity at grain-boundary surface terminations, *Science*, 2017, **358**, 1187–1192.
59 Y. Pang, *et al.*, Efficient electrocatalytic conversion of carbon monoxide to propanol using fragmented copper, *Nat. Catal.*, 2019, **2**, 251–258.
60 Q. Wu, *et al.*, Nanograin-Boundary-Abundant Cu_2O-Cu Nanocubes with High C_{2+} Selectivity and Good Stability during Electrochemical CO_2 Reduction at a Current Density of 500 mA/cm^2, *ACS Nano*, 2023, **17**(13), 12884–12894.
61 Z. Gu, *et al.*, Oxygen vacancy tuning toward efficient electrocatalytic CO_2 reduction to C_2H_4, *Small Methods*, 2019, **3**, 1800449.
62 Z. Wu, *et al.*, Grain boundary and interface interaction Co-regulation promotes SnO_2 quantum dots for efficient CO_2 reduction, *Chem. Eng. J.*, 2023, **451**, 138477.
63 J. Chen and L. Wang, Effects of the catalyst dynamic changes and influence of the reaction environment on the performance of electrochemical CO_2 reduction, *Adv. Mater.*, 2022, **34**, 2103900.
64 X. Yuan, *et al.*, Controllable Cu_0–Cu^+ sites for electrocatalytic reduction of carbon dioxide, *Angew. Chem.*, 2021, **133**, 15472–15475.
65 H. Li, *et al.*, Oxygen vacancy structure associated photocatalytic water oxidation of BiOCl, *ACS Catal.*, 2016, **6**, 8276–8285.

 This journal is © The Royal Society of Chemistry 2025

Open Access Article. Published on 23 June 2025. Downloaded on 4/15/2026 7:29:37 PM. This article is licensed under a Creative Commons Attribution-NonCommercial 3.0 Unported Licence.

66 H. Li, J. Li, Z. Ai, F. Jia and L. Zhang, Oxygen vacancy–mediated photocatalysis of BiOCl: reactivity, selectivity, and perspectives, *Angew. Chem., Int. Ed.*, 2018, **57**, 122–138.
67 Y. Wang, P. Han, X. Lv, L. Zhang and G. Zheng, Defect and interface engineering for aqueous electrocatalytic CO_2 reduction, *Joule*, 2018, **2**, 2551–2582.
68 C. Choi, *et al.*, A highly active star decahedron Cu nanocatalyst for hydrocarbon production at low overpotentials, *Adv. Mater.*, 2019, **31**, 1805405.
69 Y. Huang, A. D. Handoko, P. Hirunsit and B. S. Yeo, Electrochemical reduction of CO_2 using copper single-crystal surfaces: effects of CO* coverage on the selective formation of ethylene, *ACS Catal.*, 2017, **7**, 1749–1756.
70 D. Gao, *et al.*, Plasma-activated copper nanocube catalysts for efficient carbon dioxide electroreduction to hydrocarbons and alcohols, *ACS Nano*, 2017, **11**, 4825–4831.
71 J. Kim, *et al.*, Branched copper oxide nanoparticles induce highly selective ethylene production by electrochemical carbon dioxide reduction, *J. Am. Chem. Soc.*, 2019, **141**, 6986–6994.
72 D. Kim, C. S. Kley, Y. Li and P. Yang, Copper nanoparticle ensembles for selective electroreduction of CO_2 to C_2–C_3 products, *Proc. Natl. Acad. Sci. U. S. A.*, 2017, **114**, 10560–10565.
73 D. Wakerley, *et al.*, Bio-inspired hydrophobicity promotes CO_2 reduction on a Cu surface, *Nat. Mater.*, 2019, **18**, 1222–1227.
74 C. Reller, *et al.*, Selective electroreduction of CO_2 toward ethylene on nano dendritic copper catalysts at high current density, *Adv. Energy Mater.*, 2017, **7**, 1602114.
75 B. Thomas, P. Yuanjie, D. Cao-Thang, L. Min and S. David, *Nanomorphology-Enhanced Gas-Evolution Intensifies CO_2 Reduction Electrochemistry*, 2017.
76 M. Liu, *et al.*, Enhanced electrocatalytic CO_2 reduction via field-induced reagent concentration, *Nature*, 2016, **537**, 382–386.
77 T. Saberi Safaei, *et al.*, High-density nanosharp microstructures enable efficient CO_2 electroreduction, *Nano Lett.*, 2016, **16**, 7224–7228.
78 L. D. Chen, M. Urushihara, K. Chan and J. K. Nørskov, Electric field effects in electrochemical CO_2 reduction, *ACS Catal.*, 2016, **6**, 7133–7139.
79 D. M. Weekes, D. A. Salvatore, A. Reyes, A. Huang and C. P. Berlinguette, Electrolytic CO_2 reduction in a flow cell, *Acc. Chem. Res.*, 2018, **51**, 910–918.
80 B. Seger, M. Robert and F. Jiao, Best practices for electrochemical reduction of carbon dioxide, *Nat. Sustainability*, 2023, **6**, 236–238.
81 Z. Sun, T. Ma, H. Tao, Q. Fan and B. Han, Fundamentals and challenges of electrochemical CO_2 reduction using two-dimensional materials, *Chem*, 2017, **3**, 560–587.
82 J. Chen, *et al.*, Selective and stable CO_2 electroreduction at high rates via control of local H_2O/CO_2 ratio, *Nat. Commun.*, 2024, **15**, 5893.
83 T. Burdyny, W. A. Smith, *et al.*, CO_2 reduction on gas-diffusion electrodes and why catalytic performance must be assessed at commercially-relevant conditions, *Energy Environ. Sci.*, 2019, **12**, 1442–1453.
84 E. A. dos Reis, G. T. da Silva, E. I. Santiago and C. Ribeiro, Revisiting electrocatalytic CO_2 reduction in nonaqueous media: promoting CO_2 recycling in organic molecules by controlling H_2 evolution, *Energy Technol.*, 2023, **11**, 2201367.
85 K. Liu, W. A. Smith and T. Burdyny, Introductory guide to assembling and operating gas diffusion electrodes for electrochemical CO_2 reduction, *ACS Energy Lett.*, 2019, **4**, 639–643.
86 H.-P. Iglesias van Montfort, *et al.*, An advanced guide to assembly and operation of CO_2 electrolyzers, *ACS Energy Lett.*, 2023, **8**, 4156–4161.
87 X. Chen, *et al.*, Electrochemical CO_2-to-ethylene conversion on polyamine-incorporated Cu electrodes, *Nat. Catal.*, 2021, **4**, 20–27.
88 W. Ma, *et al.*, Electrocatalytic reduction of CO_2 and CO to multi-carbon compounds over Cu-based catalysts, *Chem. Soc. Rev.*, 2021, **50**, 12897–12914.
89 X. Lu, *et al.*, In situ observation of the pH gradient near the gas diffusion electrode of CO_2 reduction in alkaline electrolyte, *J. Am. Chem. Soc.*, 2020, **142**, 15438–15444.
90 F. P. García de Arquer, *et al.*, CO_2 electrolysis to multicarbon products at activities greater than 1 A cm^{-2}, *Science*, 2020, **367**, 661–666.
91 Q. Gong, *et al.*, Structural defects on converted bismuth oxide nanotubes enable highly active electrocatalysis of carbon dioxide reduction, *Nat. Commun.*, 2019, **10**, 2807.
92 J. C. Bui, *et al.*, Engineering catalyst–electrolyte microenvironments to optimize the activity and selectivity for the electrochemical reduction of CO_2 on Cu and Ag, *Acc. Chem. Res.*, 2022, **55**, 484–494.
93 C.-T. Dinh, *et al.*, CO_2 electroreduction to ethylene via hydroxide-mediated copper catalysis at an abrupt interface, *Science*, 2018, **360**, 783–787.
94 X. Zhang, *et al.*, Selective and high current CO_2 electroreduction to multicarbon products in near-neutral KCl electrolytes, *J. Am. Chem. Soc.*, 2021, **143**, 3245–3255.
95 C. Chen, Y. Li and P. Yang, Address the "alkalinity problem" in CO_2 electrolysis with catalyst design and translation, *Joule*, 2021, **5**, 737–742.
96 Y. Cao, *et al.*, Surface hydroxide promotes CO_2 electrolysis to ethylene in acidic conditions, *Nat. Commun.*, 2023, **14**, 2387.
97 Z. Wang, *et al.*, Localized Alkaline Environment via In Situ Electrostatic Confinement for Enhanced CO_2-to-Ethylene Conversion in Neutral Medium, *J. Am. Chem. Soc.*, 2023, **145**(11), 6339–6348.
98 W. Ma, *et al.*, Electrocatalytic reduction of CO_2 to ethylene and ethanol through hydrogen-assisted C–C coupling over fluorine-modified copper, *Nat. Catal.*, 2020, **3**, 478–487.
99 I. Merino-Garcia, J. Albo and A. Irabien, Tailoring gas-phase CO_2 electroreduction selectivity to hydrocarbons at Cu nanoparticles, *Nanotechnology*, 2017, **29**, 014001.
100 H. Xu, *et al.*, Highly selective electrocatalytic CO_2 reduction to ethanol by metallic clusters dynamically

Open Access Article. Published on 23 June 2025. Downloaded on 4/15/2026 7:29:37 PM. This article is licensed under a Creative Commons Attribution-NonCommercial 3.0 Unported Licence.

formed from atomically dispersed copper, *Nat. Energy*, 2020, **5**, 623–632.

101 Y. Liu, S. Chen, X. Quan and H. Yu, Efficient electrochemical reduction of carbon dioxide to acetate on nitrogen-doped nanodiamond, *J. Am. Chem. Soc.*, 2015, **137**, 11631–11636.

102 W. Guo, *et al.*, Highly efficient CO_2 electroreduction to methanol through atomically dispersed Sn coupled with defective CuO catalysts, *Angew. Chem., Int. Ed.*, 2021, **60**, 21979–21987.

103 W. Ren, *et al.*, Isolated diatomic Ni–Fe metal–nitrogen sites for synergistic electroreduction of CO_2, *Angew. Chem., Int. Ed.*, 2019, **58**, 6972–6976.

104 X. Hou, *et al.*, 3D core–shell porous-structured Cu@ Sn hybrid electrodes with unprecedented selective CO_2-into-formate electroreduction achieving 100%, *J. Mater. Chem. A*, 2019, **7**, 3197–3205.

105 W. Liu, *et al.*, Electrochemical CO_2 reduction to ethylene by ultrathin CuO nanoplate arrays, *Nat. Commun.*, 2022, **13**, 1877.

106 Y. Zhang, *et al.*, Low-coordinated copper facilitates the* CH_2CO affinity at enhanced rectifying interface of Cu/Cu_2O for efficient CO_2-to-multicarbon alcohols conversion, *Nat. Commun.*, 2024, **15**, 5172.

107 T. Zhang, B. Yuan, W. Wang, J. He and X. Xiang, Tailoring* H intermediate coverage on the $CuAl_2O_4$/CuO catalyst for enhanced electrocatalytic CO_2 reduction to ethanol, *Angew. Chem.*, 2023, **135**, e202302096.

108 R. Zhang, *et al.*, Synthesis of *n*-Propanol from CO_2 Electroreduction on Bicontinuous Cu_2O/Cu Nanodomains, *Angew. Chem., Int. Ed.*, 2024, **63**, e202405733.

109 M. Fang, L. Xu, H. Zhang, Y. Zhu and W.-Y. Wong, Metalloporphyrin-linked mercurated graphynes for ultrastable CO_2 electroreduction to CO with nearly 100% selectivity at a current density of 1.2 A cm^{-2}, *J. Am. Chem. Soc.*, 2022, **144**, 15143–15154.

110 L. Fan, C. Xia, P. Zhu, Y. Lu and H. Wang, Electrochemical CO_2 reduction to high-concentration pure formic acid solutions in an all-solid-state reactor, *Nat. Commun.*, 2020, **11**, 3633.

111 D. Bagchi, *et al.*, Structure–tailored surface oxide on Cu–Ga intermetallics enhances CO_2 reduction selectivity to methanol at ultralow potential, *Adv. Mater.*, 2022, **34**, 2109426.

112 J. Liu, *et al.*, Switching between C_{2+} products and CH_4 in CO_2 electrolysis by tuning the composition and structure of rare-earth/copper catalysts, *J. Am. Chem. Soc.*, 2023, **145**, 23037–23047.

113 C. Peng, *et al.*, Highly–Exposed Single–Interlayered Cu Edges Enable High–Rate CO_2-to-CH_4 Electrosynthesis, *Adv. Energy Mater.*, 2022, **12**, 2200195.

114 L. Wang, *et al.*, Stabilized $Cu^{\delta+}$-OH species on in situ reconstructed Cu nanoparticles for CO_2-to-C_2H_4 conversion in neutral media, *Nat. Commun.*, 2024, **15**, 7477.

115 L. Shang, X. Lv, L. Zhong, S. Li and G. Zheng, Efficient CO_2 electroreduction to ethanol by Cu_3Sn catalyst, *Small Methods*, 2022, **6**, 2101334.

116 Y. Xu, *et al.*, Low coordination number copper catalysts for electrochemical CO_2 methanation in a membrane electrode assembly, *Nat. Commun.*, 2021, **12**, 2932.

117 Y. Wu, *et al.*, Enhancing CO_2 electroreduction to CH_4 over Cu nanoparticles supported on N-doped carbon, *Chem. Sci.*, 2022, **13**, 8388–8394.

118 T. Zheng, *et al.*, Large-scale and highly selective CO_2 electrocatalytic reduction on nickel single-atom catalyst, *Joule*, 2019, **3**, 265–278.

119 Q. Xu, *et al.*, Enriching surface–accessible CO_2 in the zero–gap anion–exchange–membrane–based CO_2 electrolyzer, *Angew. Chem., Int. Ed.*, 2023, **62**, e202214383.

120 L. Ge, *et al.*, Electrochemical CO_2 reduction in membrane-electrode assemblies, *Chem*, 2022, **8**, 663–692.

121 C. M. Gabardo, *et al.*, Continuous carbon dioxide electroreduction to concentrated multi-carbon products using a membrane electrode assembly, *Joule*, 2019, **3**, 2777–2791.

122 Z. Gu, *et al.*, Efficient electrocatalytic CO_2 reduction to C_{2+} alcohols at defect-site-rich Cu surface, *Joule*, 2021, **5**, 429–440.

123 L. Wang, *et al.*, Interface engineering and oxygen vacancies derived from plasma-treated Cu_2O synergistically enhancing electrocatalytic CO_2-to-C_{2+} conversion, *J. Mater. Chem. A*, 2024, **12**, 21864–21872.

124 L. Wang, *et al.*, Revealing Real Active Sites in Intricate Grain Boundaries Assemblies on Electroreduction of CO_2 to C_{2+} Products, *Adv. Energy Mater.*, 2025, **15**, 2402636.

125 L. Fan, *et al.*, Strategies in catalysts and electrolyzer design for electrochemical CO_2 reduction toward C_{2+} products, *Sci. Adv.*, 2020, **6**, eaay3111.

126 M. Jouny, W. Luc and F. Jiao, High-rate electroreduction of carbon monoxide to multi-carbon products, *Nat. Catal.*, 2018, **1**, 748–755.

127 A. S. Varela, M. Kroschel, T. Reier and P. Strasser, Controlling the selectivity of CO_2 electroreduction on copper: The effect of the electrolyte concentration and the importance of the local pH, *Catal. Today*, 2016, **260**, 8–13.

128 S. Ma, *et al.*, Carbon nanotube containing Ag catalyst layers for efficient and selective reduction of carbon dioxide, *J. Mater. Chem. A*, 2016, **4**, 8573–8578.

129 X. Lu, D. Y. Leung, H. Wang, M. K. Leung and J. Xuan, Electrochemical reduction of carbon dioxide to formic acid, *ChemElectroChem*, 2014, **1**, 836–849.

130 D. S. Ripatti, T. R. Veltman and M. W. Kanan, Carbon monoxide gas diffusion electrolysis that produces concentrated C_2 products with high single-pass conversion, *Joule*, 2019, **3**, 240–256.

131 J. J. Lv, *et al.*, A highly porous copper electrocatalyst for carbon dioxide reduction, *Adv. Mater.*, 2018, **30**, 1803111.

132 Y. Wu, *et al.*, Mitigating electrolyte flooding for electrochemical CO_2 reduction via infiltration of hydrophobic particles in a gas diffusion layer, *ACS Energy Lett.*, 2022, **7**, 2884–2892.

133 K. U. Hansen and F. Jiao, Hydrophobicity of CO_2 gas diffusion electrodes, *Joule*, 2021, **5**, 754–757.

134 Z. Xing, K. Shi, X. Hu and X. Feng, Beyond catalytic materials: Controlling local gas/liquid environment in the

 This journal is © The Royal Society of Chemistry 2025

Open Access Article. Published on 23 June 2025. Downloaded on 4/15/2026 7:29:37 PM.
This article is licensed under a Creative Commons Attribution-NonCommercial 3.0 Unported Licence.

catalyst layer for CO_2 electrolysis, *J. Energy Chem.*, 2022, **66**, 45–51.

135 Z. Xing, L. Hu, D. S. Ripatti, X. Hu and X. Feng, Enhancing carbon dioxide gas-diffusion electrolysis by creating a hydrophobic catalyst microenvironment, *Nat. Commun.*, 2021, **12**, 136.

136 M. Li, *et al.*, The role of electrode wettability in electrochemical reduction of carbon dioxide, *J. Mater. Chem. A*, 2021, **9**, 19369–19409.

137 J. Bi, *et al.*, Construction of 3D copper-chitosan-gas diffusion layer electrode for highly efficient CO_2 electrolysis to C_{2+} alcohols, *Nat. Commun.*, 2023, **14**, 2823.